University of Bath

STA-27, a porous scandium MOF with an unexpected topology type prepared with the tetracarboxyphenylpyrazine linker

Ram. R. R. Prasad,[a] Sarah E. Seidner,[a] David B. Cordes,[a] Magdalena M. Lozinska,[a] Daniel M. Dawson,[a] Megan J. Thompson,[b] Tina Düren,[b] Kristina K. Chakarova,[c] Konstanin I. Hadjiivanov,[c] Alexandra M. Z. Slawin,[a] Sharon. E. Ashbrook,[a] Matthew L. Clarke [a] and Paul A. Wright[a]*

[a] EaStCHEM School of Chemistry, University of St Andrews, Purdie Building, North Haugh, St Andrews, KY16 9ST, UK
[b] Centre for Advanced Separations Engineering, Department of Chemical Engineering, University of Bath, Bath, BA2 7AY, UK
[c] Institute of General and Inorganic Chemistry, Bulgarian Academy of Sciences, Sofia 1113, Bulgaria

E-mail : paw2@st-andrews.ac.uk

Abstract: A porous scandium MOF denoted STA-27 (St Andrews Porous Material-27) has been synthesised solvothermally using 2,3,5,6-tetrakis(4-carboxyphenyl)pyrazine (TCPP) as the tetratopic carboxylate linker. STA-27 possesses a unique type of 1D rod-based secondary building unit (SBU) with corner-sharing scandium dimers connected via carboxylate groups from the TCPP. Under similar synthesis conditions the smaller Al^{3+} and Ga^{3+} cations give a predictable MOF-topology type based on chains of corner-sharing $MO_4(OH)_2$ octahedra. After activation under mild conditions STA-27 is an active Lewis acidic catalyst, while heating at elevated temperatures results in rupturing of the Sc-O-Sc linkages and a phase transition to a different topological type**.**

Introduction

Reticular chemistry, the underlying principle of which is the designed assembly of metal cation-based nodes and polytopic organic linkers, has been used to great effect in the preparation of numerous families of porous metal organic frameworks (MOFs).[1-5] Among these, the carboxylates MIL-53,[6] -88,[7] -100,[8] -101,[9] soc-MOF[10] and MFM-300[11] of the trivalent metal cations Al^{3+}, Cr^{3+}, Fe^{3+} and Ga^{3+} are some of the most intensely studied MOFs for potential applications in adsorption, separation, drug delivery and catalysis. In these materials, the metal-cation based inorganic nodes take the form of corner-sharing chains or trimers of MO_6 octahedra, as shown in Figure 1.

It is also possible to prepare Sc^{3+} analogues of these carboxylate MOFs, where the slightly larger Sc^{3+} cations (0.745 Å vs 0.675 Å (Al^{3+})) adopt octahedral coordination in their chain or trimer building units, modifying the breathing behaviour of MIL-53 and imparting highly effective Lewis acidic catalytic sites to MIL-100, for example.[12] Additionally, it is possible to prepare porous MOFs with Sc^{3+} within the metal nodes that are structurally different from those prepared with the other cations, due to its larger radius.[13-15] These include Sc_2BDC_3, a highly stable MOF which displays a unique set of properties for the adsorption of small molecules such as CO_2 and small alkanes that has not been prepared for metals other than with scandium.[14] Given the attractive properties for adsorption and catalysis reported above, the area of Sc MOFs remains relatively less studied so that the investigation of tetracarboxylate Sc-MOFs seemed particularly timely, as only two had been reported, NOTT-401[16] and the Sc analogue of In-socMOF[12a,c]. 2,3,5,6-tetrakis(4-carboxyphenyl)pyrazine (TCPP, Figure 3) is a readily-prepared and flexible linker that had only been reported rarely in MOF synthesis,[17] that we felt might produce useful tetracarboxylate Sc MOFs.
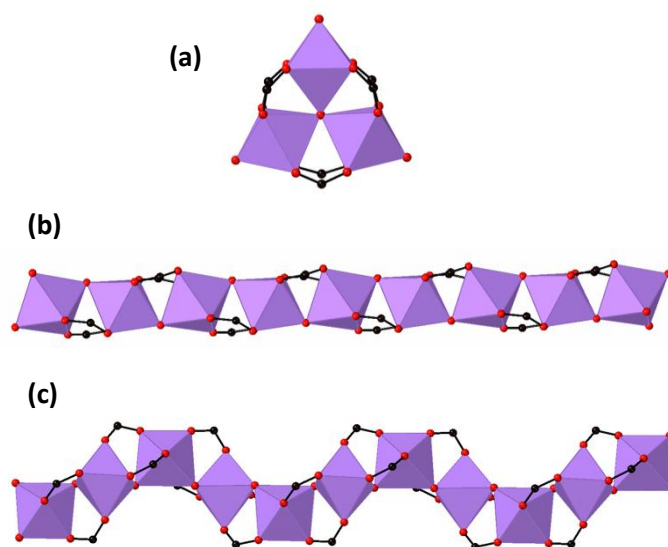
Figure 1: Popular SBUs in M^{3+} based MOFs: a) Trimer based SBUs of MIL-88, -100, -101 and soc MOFs, b) 1D rod SBU of MIL-53 family and c) 1D rod SBU of MFM-300.

Here we describe the results of syntheses of TCPP-based MOFs with Sc^{3+}, as well as with the trivalent metal cations Al^{3+} and Ga^{3+} for comparison. While the latter two cations give structural analogues of the reported Al-MOF, $[Al_2(OH)_2(TCPB)]^{18}$ prepared

from the similar linker 2,3,5,6-tetrakis(4-carboxyphenyl)benzene (TCPB, Figure 3), as might have been predicted by reticular chemistry, the use of Sc^{3+} results in STA-27, a microporous 3D-connected scandium MOF with an unprecedented infinite rod building unit. We describe its adsorptive and Lewis acidic catalytic properties and report that it undergoes a structural phase transition at elevated temperature.

Experimental

Synthesis of TCPP

TCPP was synthesised in two steps by modifying the reported procedure.[17] The synthesis procedure and details of its characterization are given in the ESI.

Synthesis of Al$_2$(OH)$_2$TCPP

Al$_2$(OH)$_2$TCPP was synthesised in a mixed solvent system of N, N-dimethylformamide (DMF) and nitric acid (HNO_3). 190.6 mg Al(NO$_3$)$_3$.9H$_2$O or 216. mg AlCl$_3$.6H$_2$O (0.895 mmol) and 41.2 mg TCPP (0.074mmol) were weighed out into a Teflon-liner equipped (total volume ~ 30mL) containing a magnetic stirrer bar. 7.5 mL of DMF followed by 7.5 mL of 3.5 M aq. HNO_3 were added to the mixture using either a syringe or measuring cylinder. The solution was stirred at room temperature until it turned pale yellow (usually 45-50 min). The stirrer bar was removed, and the Teflon-liner was placed inside a stainless-steel autoclave before heating in a pre-heated oven at 150 °C for 30 h. After cooling to room temperature at a rate of 5 °C/min. The resulting white powder was filtered and washed multiple times with DMF followed by methanol and kept in methanol overnight before filtering and drying at 80 °C overnight.

Synthesis of Ga$_2$(OH)$_2$TCPP

Ga$_2$(OH)$_2$TCPP was synthesised in DMF and HNO_3 similarly to Al$_2$(OH)$_2$TCPP. 228.8 mg Ga(NO$_3$)$_3$.xH$_2$O (0.895 mmol) and 41.2 mg TCPP (0.074mmol) were weighed out into a Teflon-liner equipped (total volume~30mL) with a magnetic stirrer bar. 7.5 mL of DMF followed by 3.5 M aq. HNO_3 was added to the mixture using either a syringe or measuring cylinder. The solution was stirred at room temperature until the colour of the solution changed to pale yellow (usually 45-50 min). The stirrer bar was removed, and the Teflon-liner was placed inside a stainless-steel autoclave before heating in a pre-heated oven at 150 °C for 40 h. After cooling to room temperature at a rate of 5 °C/min, the single crystals of Ga-TCPP obtained was filtered and washed multiple times DMF with followed by methanol and kept in methanol overnight before filtering and drying at 80 °C overnight.

Synthesis of STA-27, $Sc_2(O)(H_2O)_2TCPP$

STA-27 was synthesised using a mixed solvent system of DMF, aq: HNO_3 and acetonitrile with $ScCl_3.6H_2O$ and TCPP as the precursors. 232.4 mg $ScCl_3.6H_2O$ (0.895 mmol) and 41.2 mg TCPP (0.074mmol) was weighed out into a Teflon-liner equipped (Total volume~30mL) with a magnetic stirrer bar. 7.5 mL of DMF followed by 7.5 mL of 3.5 M aq. HNO_3 and 7.5 mL acetonitrile was added to the mixture using either a syringe or measuring cylinder. The solution was stirred at room temperature until the colour of the solution changed to pale yellow (usually 45-50 min). The stirrer bar was removed, and the Teflon-liner was placed inside a stainless-steel autoclave before heating in a pre-heated oven at 150 °C for 30 h. After cooling to room temperature at a rate of 5 °C/min, convex shaped single-crystals of STA-27. The crystals were washed multiple times with DMF and followed by methanol and kept in methanol overnight before filtering and drying at 80 °C overnight. CHN analysis : Calculated- C, 49.33; H, 3.42; N, 5.49. Found- C, 49.37; H, 3.33; N, 5.49.

Characterisation

Powder X-ray diffraction (PXRD) patterns on finely ground MOF samples were collected in Debye-Scherrer geometry on Stoe STAD i/p diffractometers with primary monochromation (Cu $K_{\alpha1,}$ λ = 1.54056 Å), using either 0.5 or 0.7 mm glass capillaries. Variable temperature PXRD (VT-PXRD) measurements for STA-27 were performed in open quartz capillaries in a flow of dry nitrogen flow with a ramp rate of 5 °C min^{-1} and held at the desired temperature for 10 min prior to measurements. Data were collected from 25 to 225 °C and after cooling down to 25 °C using a Cobra Plus non-liquid-nitrogen cryostream (Oxford Cryosystems).

Single crystal X-ray diffraction (SCXRD) data for STA-27 and $Ga_2(OH)_2(TCPP)$ were collected at 173 K using a Rigaku MM-007HF High brilliance RA generator/confocal optics and Rigaku XtaLAB P100 system, with Cu K α radiation (λ = 1.54187 Å). Intensity data were collected using both ω and ϕ steps, accumulating area detector images spanning at least a hemisphere of reciprocal space. Data were corrected for Lorentz polarization effects, and a multiscan absorption correction was applied by using CrystalClear.[19] Structures were solved by dual-space methods (SHELXT),[20] and refined by full-matrix least-squares against F^2 (SHELXL-2016/6).[21] Non-hydrogen atoms were refined anisotropically, and alkyl and aryl hydrogen atoms were refined using a riding model.

Terminal oxygens were identified as water for STA-27, although hydrogen atoms could not be located. All calculations were performed using the CrystalStructure[22] interface. The data showed non-merohedral twinning (twin law 1 0 0.313 0 -1 0 0 0 -1, twin fraction 47 %), which was accounted for in the refinement. STA-27 structure showed large voids, 1069 $Å^3$ 46.5 % of unit cell volume, and the SQUEEZE[23] routine implemented in PLATON[24] was used to remove the contribution of the unordered electron density in the void spaces.

Solid-state NMR (SS-NMR) spectra were recorded using a Bruker Avance III spectrometer equipped with a 9.4 T superconducting magnet (Larmor frequencies of 400.1 MHz for ^1H, 100.6 MHz for ^{13}C and 97.2 MHz for ^{45}Sc). Samples were packed into standard ZrO_2 rotors with outer diameters of 4 mm and rotated at the magic angle at a rate of 12.5 kHz (^{13}C) or 14 kHz (^{45}Sc). The ^{13}C NMR spectrum was recorded with cross polarisation (CP) from ^1H with a contact pulse (ramped for ^1H) of 2 ms. Signal averaging was carried out for 4096 transients with a recycle interval of 3 s. Two-pulse phase modulation (TPPM) decoupling of ^1H ($n_1 \approx$ 100 kHz) was carried out during acquisition. For the ^{45}Sc NMR spectra, signal averaging was carried out for 1024 transients with a recycle interval of 0.25 s. The ^{45}Sc multiple-quantum (MQ) magic angle spinning (MAS) spectrum was recorded using a z-filtered pulse sequence and then sheared and referenced according to Pike *et al.*[25] Signal averaging was carried out for 5664 transients for each of 20 t_1 increments of 35.7 ms with a recycle interval of 0.25 s. Chemical shifts are reported in ppm relative to TMS (^{13}C) or 0.06 M $Sc(NO_3)_3$ in D_2O (^{45}Sc), using L-alanine (**C**H_3 δ = 20.5 ppm) and $LaScO_3$ (δ= 162 ppm) as secondary solid references.

Thermogravimetric analysis (TGA) of all MOF samples were carried out on a Netzsch TGA 760 for a temperature range of 20 - 800 °C at a heating rate of 5 °C min^{-1} in a continuous air flow. N_2 adsorption isotherms for all the MOFs were measured volumetrically on a Micrometrics Tristar at -196 °C. The CO_2 adsorptions isotherms were measured gravimetrically on Hiden IGA porosimeter at room temperature. All samples were activated at 150 °C prior to measurements.

The FTIR spectra were recorded with Nicolet Avatar 360 and Nicolet 6700 FTIR spectrometers accumulating 64 scans at a spectral resolution of 2 cm^{-1} and accuracy of 0.01 cm^{-1}. The IR measurements of STA-27 were made with *(i)* MOF samples spread on the surface of preliminary pressed KBr discs and *(ii)* self-supporting pellets. The pellets were treated directly in a specially designed IR cell allowing measurements at ambient and low (100 K) temperatures. The cell was directly connected to a vacuum-adsorption apparatus with a

residual pressure lower than 10^{-3} Pa. The IR experiments were made *in-situ* with as-prepared (air exposed) samples and samples activated by outgassing under high vacuum (~ 10^{-6} mbar) at ambient and elevated temperatures.

Grand canonical Monte Carlo simulations were carried out using the general-purpose molecular simulation code MuSiC.[26] The Lennard-Jones (LJ) parameters for the framework atoms were taken from the Dreiding forcefield,[27] with the exception of Scandium; the parameters for which were taken from the Universal forcefield.[28] Dinitrogen LJ parameters were taken from the Transferable Potentials for Phase Equilibria (TraPPE) forcefield.[29] Lorentz-Berthelot mixing rules were applied for LJ interactions between different atom types, and interactions between atoms separated by a distance greater than the cut-off radius of 18 Å were truncated. GCMC moves implemented on the N_2 molecules (insertion, deletion, translation and rotation) were carried out with equal weighting. For each pressure point, 10 million iterations were used, 40 % of which were used for equilibration.

Table 1. Crystallographic data for $Ga_2(OH)_2TCPP$, STA-27 and STA-27-*C*			
Parameter	$Ga_2(OH)_2TCPP$	STA-27	STA-27-*C*
Formula	$C_{32}H_{16}N_2O_8Ga_2$	$C_{32}H_{20}N_2O_{11}Sc_2$	$C_{32}H_{16}N_2O_8Sc_2$
Formula weight/g mol^{-1}	695.91	698.42	646.39
Temperature/K	93	173	173
Crystal System	Orthorhombic	Monoclinic	Orthorhombic
Space group	*Cmmm*	*P2/c*	*Pmna*
a/Å	6.68115(16)	15.504(7)	32.741(4)
b/Å	21.2861(4)	9.443(4)	7.797(3)
c/Å	15.9030(3)	15.975(7)	8.763(3)
V/Å	2261.66(8)	2308.2(18)	2237.0(12)
Z	4	2	2
ρ(calcd) g cm^{-3}	2.044	1.005	0.960
Radiation type	Mo Kα	Cu Kα	Cu Kα
μ mm^{-1}	2.454	2.910	2.920
F(000)	1392	712	656
Rint	0.0219	0.1396	0.5431
GOF	3.159	1.560	1.273
Final R1 values [I>2σ(I)]^a	0.1049	0.1409	0.1672
Final wR2 values (all data)^b	0.3518	0.4218	0.3752

Results and Discussion

Inspired by the synthesis conditions employed for isoreticular Al-Soc-MOFs by Alezi *et al.*[10d] using a tetracarboxylic acid and a metal:linker ratio of 12:1, the optimised solvothermal crystallisations (Table 2) in DMF and 3.5 M aq. HNO_3 using the TCPP linker and either $Al(NO_3)_3.9H_2O$ ($AlCl_3.6H_2O$) or $Ga(NO_3)_3.xH_2O$ as metal sources gave products containing crystalline $Al_2(OH)_2TCPP$ or $Ga_2(OH)_2TCPP$, respectively (Figure S2, S3).

Table 2: Optimising synthesis conditions for $Al_2(OH)_2TCPP$ and $Ga_2(OH)_2TCPP$							
Metal Source	Linker	DMF (mL)	HNO_3 (3.5M) (mL)	CH_3CN (mL)	Temperature (°C)	Time (h)	Phase Purity
$Al(NO_3)_3.9H_2O$	TCPP	7.5	7.5	7.5	150	30	Unknown Impurity
$Al(NO_3)_3.9H_2O$	TCPP	7.5	-	-	150	30	Amorphous
$Al(NO_3)_3.9H_2O$	TCPP	7.5	-	7.5	150	30	Impurity
$Al(NO_3)_3.9H_2O$	TCPP	7.5	7.5	-	150	30	$Al_2(OH)_2TCPP$
$Al(Cl)_3.6H_2O$	TCPP	7.5	7.5	-	150	30	$Al_2(OH)_2TCPP$
$Ga(NO_3)_3.xH_2O$	TCPP	7.5	7.5	-	150	30	$Ga_2(OH)_2TCPP$+impurity
$Ga(NO_3)_3.xH_2O$	TCPP	7.5	7.5	-	150	16	Unknown Impurity
$Ga(NO_3)_3.xH_2O$	TCPP	7.5	7.5	-	150	35	$Ga_2(OH)_2TCPP$+impurity
$Ga(NO_3)_3.xH_2O$	TCPP	7.5	7.5	-	150	40	Mostly pure $Ga_2(OH)_2TCPP$
$Ga(NO_3)_3.xH_2O$	TCPP	7.5	7.5	-	150	48	$Ga_2(OH)_2TCPP$+impurity
$Ga(NO_3)_3.xH_2O$	TCPP	7.5	7.5	-	150	48	$Ga_2(OH)_2TCPP$+Impurity
$Ga(NO_3)_3.xH_2O$	TCPP	7.5	7.5	-	150	72	$Ga_2(OH)_2TCPP$+Impurity
$Ga(NO_3)_3.xH_2O$	TCPP	7.5	7.5	-	150	96	Unknown Impurity

The $Ga_2(OH)_2TCPP$ synthesis yielded large single crystals suitable for structure solution by laboratory SCXRD as described in the Experimental Section and Table 1. The Al and Ga MOFs have very similar structures, illustrated in Figure 2 by the structure of the Ga analogue. They are isostructural with the $Al_2(OH)_2TCPB$ MOF reported by Krüger et al., the structure of which was solved from PXRD and computational modelling.[18] The difference between the TCPP and TCPB structures is that in former material the CH groups of the central benzene ring in TCPB are replaced by N atoms (Figure 3). In all these structures, the metal-based inorganic node is the infinite $MO_4(OH)_2$ chain of

corner-sharing MO_6 octahedra linked by μ_2OH groups. ^{27}Al MAS NMR and MQ (multiple-quantum) MASNMR of as-synthesised $Al_2(OH)_2TCPP$ reveals a single resonance with a typical qudrapolar line shape (Figure 4, Figure S1) similar to what was observed for MIL-53(Al).[30]

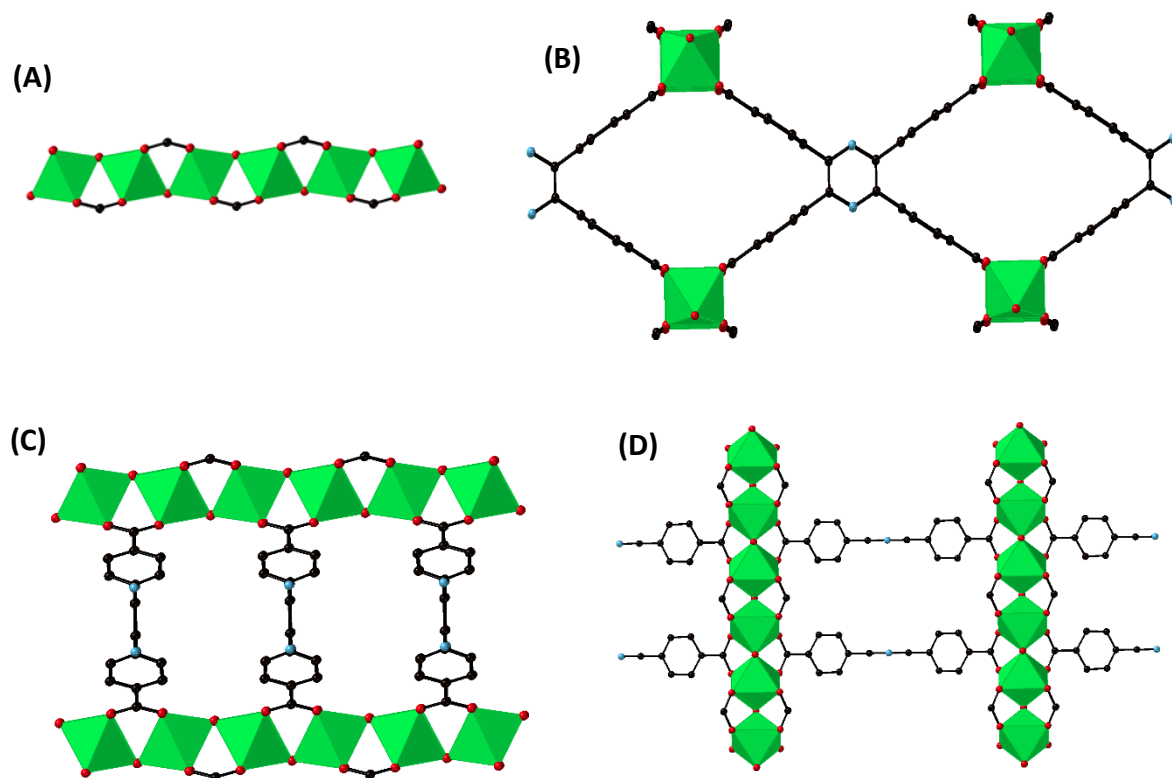**Figure 2:** Crystal Structure of $Ga_2(OH)_2TCPP$. A) 1D rod SBUs made up of corner sharing GaO_6 octahedras, B) larger pores of $Ga_2(OH)_2TCPP$ when viewed along z-axis, C) pore windows when viewed along the x-axis and D) pore windows when viewed along the y-axis. $Al_2(OH)_2TCPP$ is isostructural $Ga_2(OH)_2TCPP$ with GaO_6 octahedras replaced with AlO_6. Hydrogen atoms are omitted from the structure for clarity. Colour codes: Ga, green; N, Sky; C, Black, O; red.
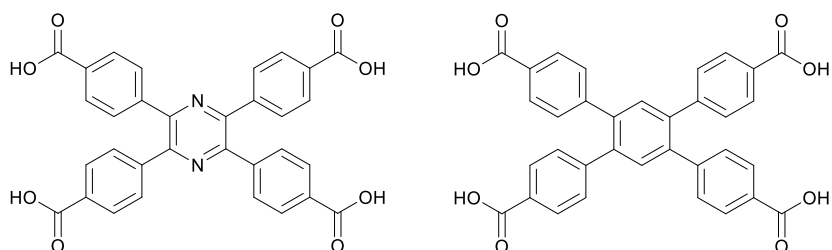

Figure 3: Structure of the linker TCPP (left) and TCPB(right). The TCPP has a pyrazine core instead of benzene for TCPB.

The $MO_4(OH)_2$ chain is the same type as that is observed in MIL-53 type MOFs,[6] but in this case the MOFs are rigid (Ga-O bond distance of 1.983 Å and Ga-OH bond distance of 1.898 Å). Each chain is linked to eight others by the TCPP linkers, the carboxylate groups of which bridge adjacent metal cations in each chain. The four phenyl rings attached to the central pyrazine group are rotated at 90° to the plane of the pyrazine, planar with their carboxylate groups. Solid-state ^{13}C CP MAS NMR gives only a single resonance for each of the chemically distinct carbon atoms of the TCPP linker as expected from the crystal symmetry of the structure (Figure 4).
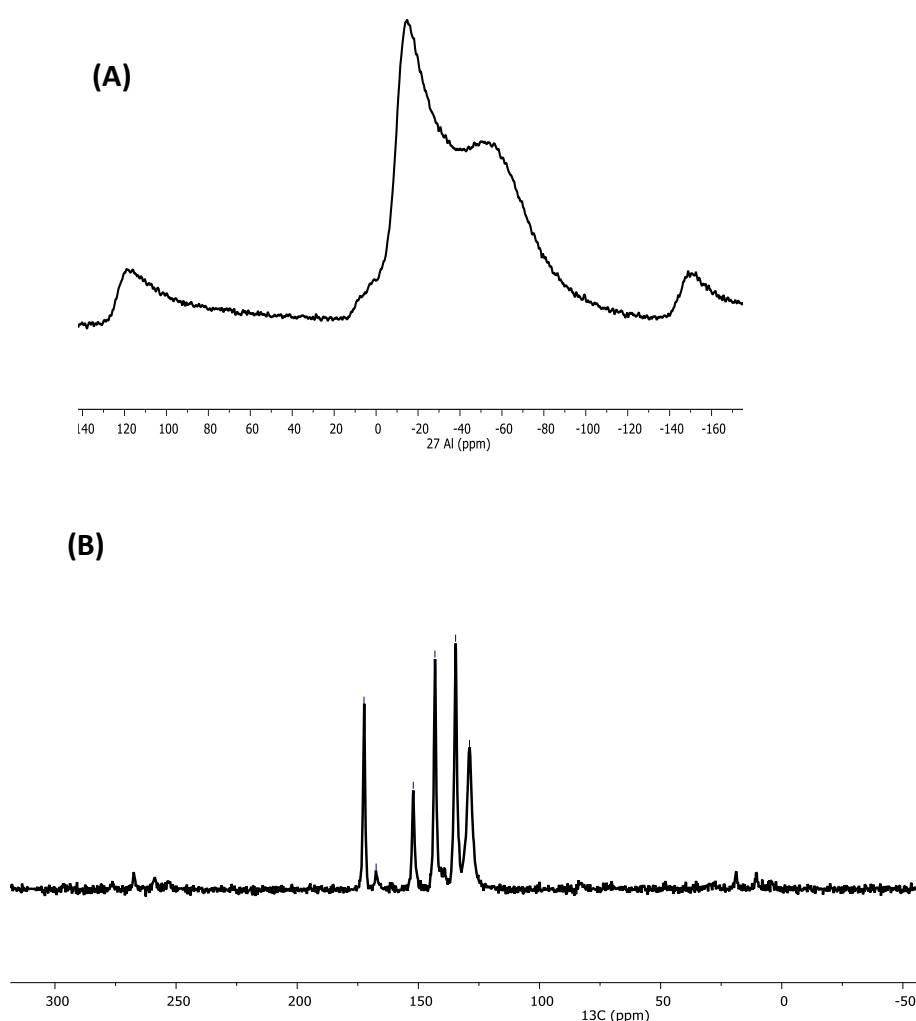

Figure 4: (A) ^{27}Al NMR of $Al_2(OH)_2TCPP$ and (B) ^{13}C CP MAS NMR spectra $Al_2(OH)_2TCPP$ showing single resonance for chemically distinct and crystallographically equivalent carbon atoms of the linker TCPP. Peaks marked with asterisk are spinning side bands.

Comparison of the experimental PXRDs of our materials with those simulated from the single crystal structure of $Ga_2(OH)_2TCPP$ indicates that the Al phase has been prepared pure while the Ga phase contains a small amount of an unidentified impurity (Figure 5A). SEM images of $Al_2(OH)_2TCPP$ (Figure 5B) showed lozenge shaped crystals while SEM images $Ga_2(OH)_2TCPP$ (Figure S4) showed crystallite of different shapes confirming the presence of impurity. We therefore concentrated on measuring properties of the pure Al phase. Notably, the previously reported $Al_2(OH)_2TCPB$ preparations contained some pseudo-boehmite impurity in all cases as detected by ^{27}Al MAS NMR, which are not present $Al_2(OH)_2TCPP$ (Figure 4, Figure S1).
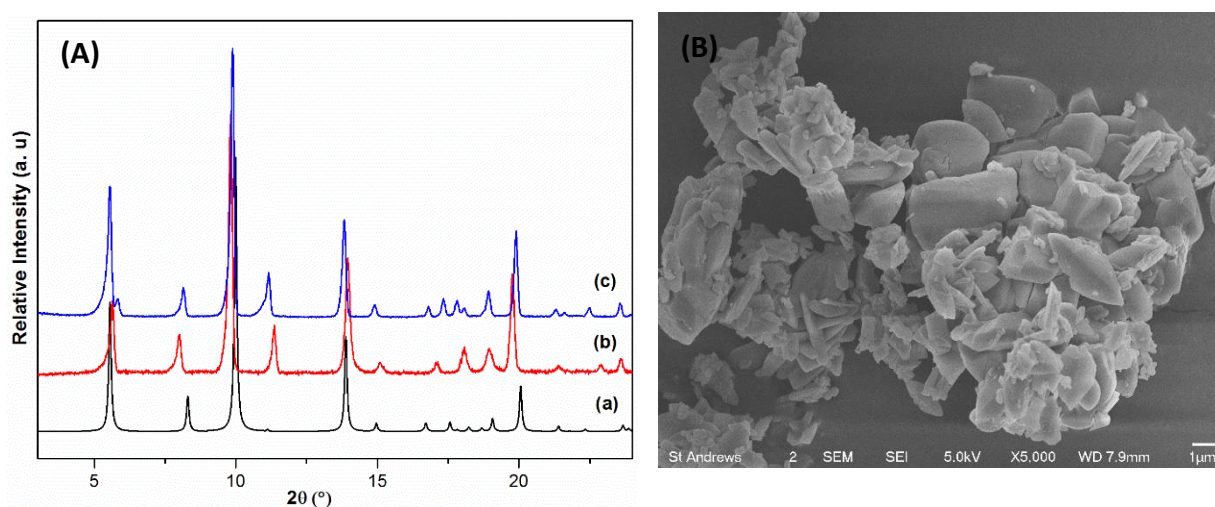

Figure 5: (A) Simulated pattern of (a) $Ga_2(OH)_2TCPP$ compared with the PXRD patterns of (b)as-synthesised $Al_2(OH)_2TCPP$ and (c) as-synthesised $Ga_2(OH)_2TCPP$ and (B) SEM image of $Al_2(OH)_2TCPP$.

TGA of as-synthesised samples of $Al_2(OH)_2TCPP$ carried out in air indicated an initial weight loss of 26 % attributed to the evaporation of adsorbed solvent molecules residing in the pores. The framework was found to be stable up to 500 °C before linker degradation leads to structural disintegration (Figure 6A). N_2 adsorption at -196 °C gave a type I isotherm (Figure 6B), as predicted from the structure, with an uptake at $P/P^o = 0.1$ of 12.4 mmol g^{-1} (corresponding to a pore volume of 0.43 cm^3 g^{-1}) and a BET surface area of 1136 m^2 g^{-1}. This compares well with the 1118 m^2 g^{-1} (pore volume of 0.43 cm^3 g^{-1}) corrected specific surface area for the $Al_2(OH)_2TCPB$ phase by Krüger et al. after taking the boehmite impurity in that preparation into account.[18] The material was also investigated for its CO_2 uptake, because the availability and low toxicity of Al, the ease of synthesis of the linker and the presence of accessible hydroxyl and amine

groups of the MOF suggested potential application as a practical adsorbent. The uptake of CO_2 at 25 °C reached 3 mmol g^{-1} at 1 bar and 6.2 mmol g^{-1} at 5 bar, showing full reversibility and no hysteresis upon desorption (Figure 6C). This value is slightly higher than large pore Al-soc-MOF under similar conditions.[10d] (No CO_2 adsorption has been reported for $Al_2(OH)_2TCPB$).
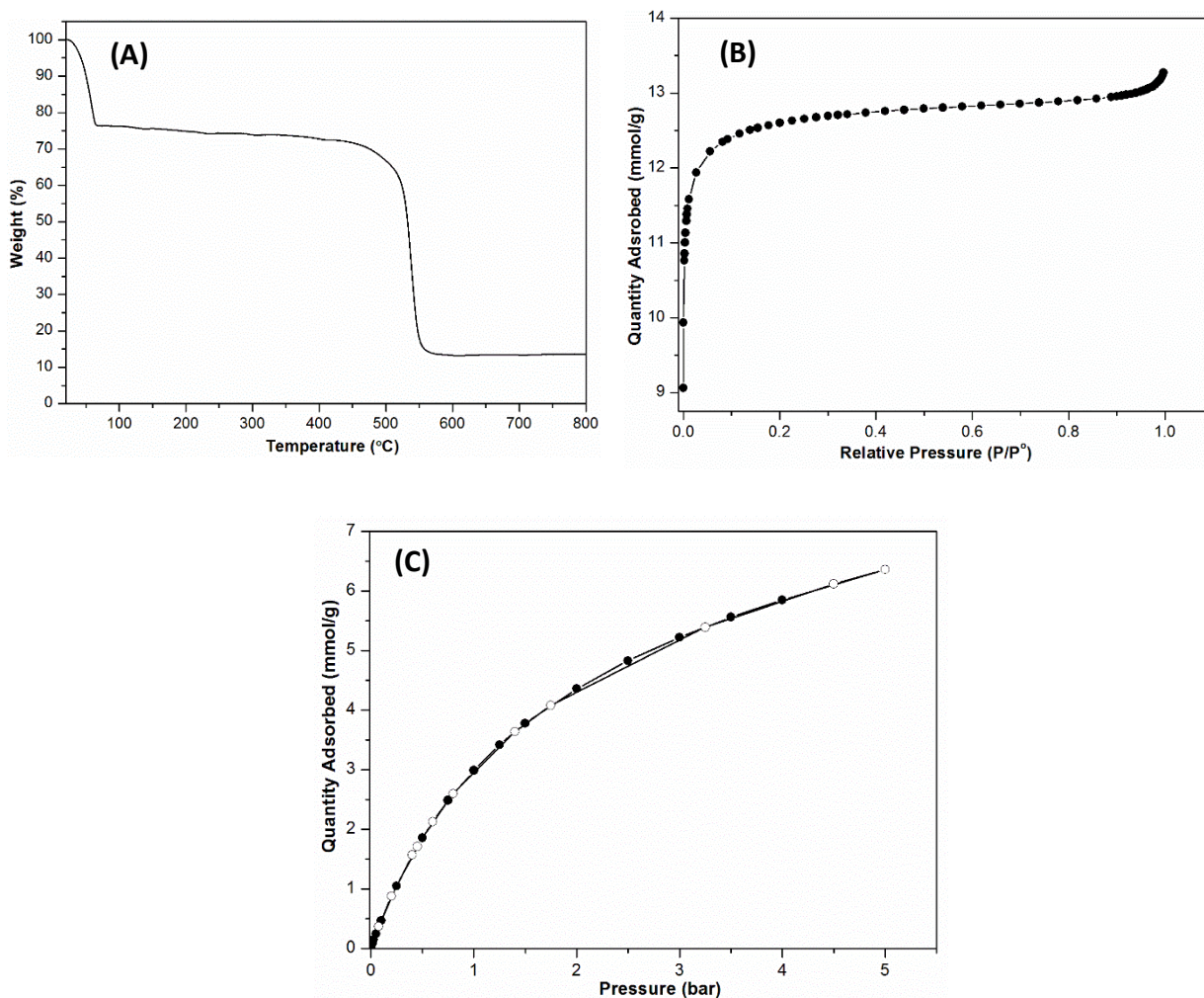

Figure 6: (A) TGA of $Al_2(OH)_2TCPP$, (B) N_2 adsorption isotherm at -196 °C for $Al_2(OH)_2TCPP$ and (C) CO_2 adsorption isotherm at 25 °C for $Al_2(OH)_2TCPP$.

When moving to the Sc-TCPP synthesis system, employing the same metal: linker ratio, changing the metal source to $ScCl_3.6H_2O$ and varying the solvent mix did not give a scandium analogue of the $Al_2(OH)_2(TCPP)$ and $Ga_2(OH)_2(TCPP)$ phases reported above, but instead gave the distinct STA-27 phase under a relatively narrow set of conditions (Table ST1). Using $ScCl_3.6H_2O$ and TCPP as precursors, with metal:linker ratio of 12:1 and a mixed solvent system of DMF, CH_3CN and 3.5 aq. HNO_3 (molar ratio

11

Sc:TCPP:DMF:CH$_3$CN:HNO$_3$ = 12:1:1311:1946:1608), heating at 150 °C gave phase pure microcrystalline STA-27 after 16 h. Extending the heating time to 30 h gave lozenge-shaped single crystals of STA-27 suitable for structure solution by laboratory SCXRD (Figure 6A). The experimental PXRD pattern for the bulk sample of STA-27 showed excellent agreement with the pattern simulated from the solved structure, confirming its phase purity (Figure 6B).
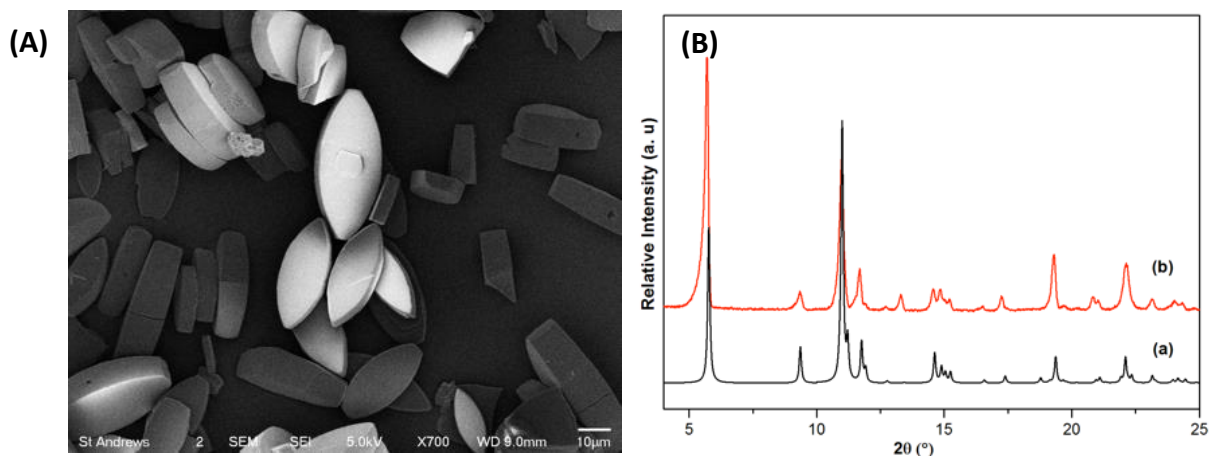

Figure 7: (A) SEM image of lozenge-shaped single crystals of STA-27. (B) Simulated pattern of (a) STA-27 compared with the PXRD pattern of (b) as-synthesised STA-27.

STA-27 displays monoclinic crystal symmetry (a = 15.5040 Å, b = 9.4430 Å, c = 15.9750 Å, β = 99.277°) with infinite rods containing octahedrally-coordinated scandium cations running along the z axis, bridged by TCPP linkers, giving rise to two different diamond-shaped channels parallel to the z axis (Figure 8C). The rods are made up of Sc$_2$O$_{11}$ dimers linked to one another via carboxylate groups (Figure 8A). Each Sc$_2$O$_{11}$ dimer comprises two corner-sharing ScO$_6$ octahedra related by symmetry, the six O atoms of each of which include four from the TCPP linkers (Sc-O distances of 2.041 Å, 2.071 Å, 2.076 Å and 2.080 Å), one bridging μ$_2$O atom (Sc-O = 2.039 Å) and one O atoms of a terminal ligand (Sc-O = 2.097 Å). Charge balance requirements of the Sc$_2$O$_{11}$ dimer suggest that if the μ$_2$O is unprotonated, the two terminal ligands are water molecules, giving an empirical formula of Sc$_2$O(H$_2$O)$_2$TCPP. Sc$_2$O$_{11}$ units have been reported previously in the scandium succinate by Perles *et al.,*[31] where the Sc in each octahedron was coordinated to five carboxylate O atoms and a shared μ$_2$OH group, but in that case

the two Sc cations in the dimer were also connected by a single succinate linker. A similar rod-like SBU to that of STA-27 was reported for an actinide MOF[32] but not to our knowledge in transition or main group metal-based MOFs.
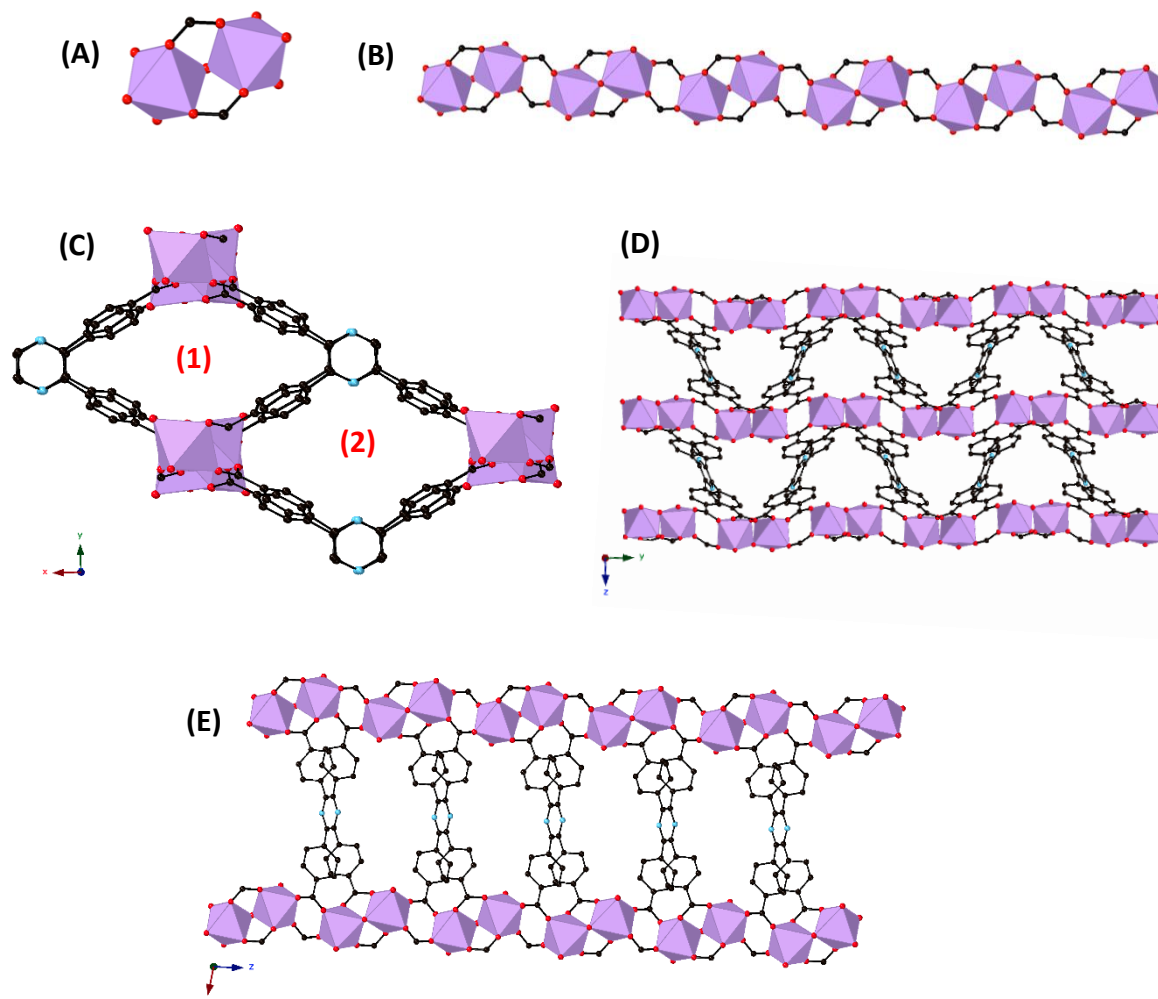

Figure 8: Crystal structure of STA-27. (A) Sc_2O_{11} dimer of STA-27, (B) 1D rod SBU of STA-27 made up of connected Sc_2O_{11} dimers, (C) two distinct diamond shaped pore channels of STA-27 viewed along the z-axis, (D) STA-27 connected via TCPP viewed along x-axis, (E) rod SBUs of STA-27 connected via TCPP viewed along y-axis. Hydrogen atoms are omitted for clarity. Colour codes: Sc, Lavender; N, Sky; C, Black, O; red.

Each TCPP linker in STA-27 is bound to four different rod SBUs, when one set of diagonally opposite carboxylate groups of the linker connects ScO_6 octahedras to Sc_2O_{11} dimer in two parallel rods, the other set connects the dimers to form rods in the other parallel pair of rod SBUs. As a consequence, the benzoate groups of TCPP are rotated at 50° to its central planar pyrazine core. The resulting diamond-shaped channels of the structure are of two types, 1 and 2, of Figure 8C. In type 1, the narrower opening (6.6 Å) of the channel (viewed down z) separates dimers of two rods, while the wider (13.5Å) is between two pyrazine rings, while in

the type 2 channels, the shorter distance (7.0 Å) is between the N atoms of pyrazine rings while the longer (10.9 Å) is between the Sc-based rods. Measured from the crystal structure, 1 and 2 channels are connected via narrow openings of 2.5 Å while the openings between adjacent channels of type 2 are only 2 Å, but rotation of the relevant benzoate group phenyl rings could increase this.

[45]Sc is a 100% abundant nucleus (I=7/2) and so Sc MOFs can be analysed by [45]Sc MAS NMR to understand the Sc coordination enviornment.[12,14,15] . [45]Sc MAS NMR gives a single resonance with an isotropic chemical shift of 39 ppm (Figure 9A) as determined by a combination of MQ MASNMR and peak shape matching, which is intermediate between the values of ScOH chains (δ = 55-62 ppm) and Sc_3O trimers (δ = 61-65 ppm) on the one hand and isolated ScO6 octahedra (Sc_2BDC_3, δ = 4 ppm) on the other. A plot of the average quadrupolar product against isotropic chemical shift (Figure 9B) distinguishes the local Sc environments according to their NMR characteristics. (Figure S5).
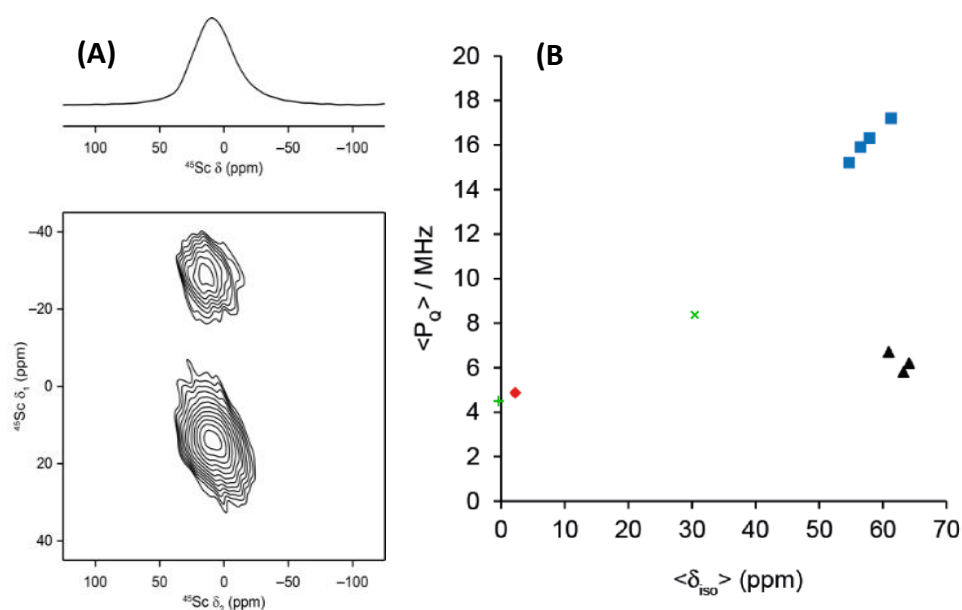

Figure 9: (A) [45]Sc MAS NMR and MQ MAS NMR spectra of STA-27 and (B) Plot of mean [47]Sc isotropic shift <δ_{iso}> and quadrupolar product <P_Q> for a series of Sc-containing MOFs with different Sc coordination motifs.[33] Red diamond = isolated ScO_6 octahedra (Sc_2BDC_3 and derivatives), blue squares = chains of ScO_6 octahedra (MIL-53 and derivatives) and black triangles = trimers of ScO_6 octahedra (MIL-88, MIL-100 and Sc-ABTC, ABTC = 3,3´,5,5´-azobenzenetetracarboxylate). Points for STA-27 are shown in green before (×) and after (+) heating. Reference points were obtained from multiple-quantum (MQ) MAS experiments carried out at 20.0 T, whereas spectra for STA-27 were recorded at 9.4 T as described in the experimental details.

TGA of as-synthesised STA-27 showed an initial mass loss of 8% attributed to the simultaneous evaporation of solvent molecules residing in the pores and water molecules attached to the clusters. Another mass loss of 7% was observed around 150 °C to 200 °C corresponding to the removal of DMF from the pores and possibly water from the ScO_6 octahedra.[34] (Figure 10).
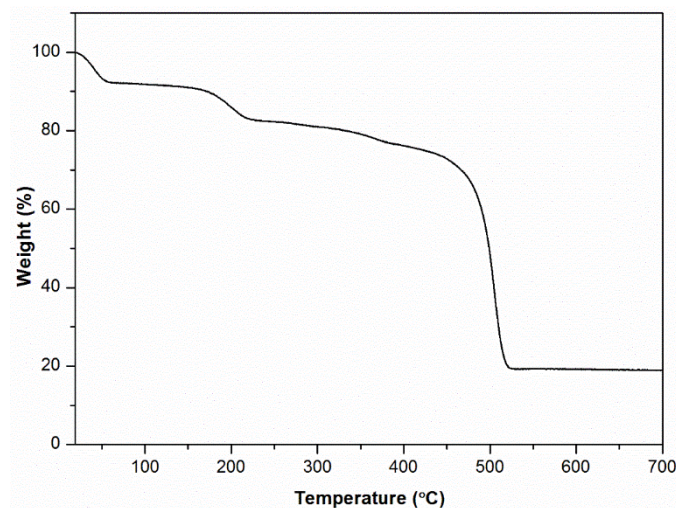

Figure 10: TGA of as-synthesised STA-27.

The response of STA-27 to heating was also studied by VT-PXRD and IR spectroscopy. VT-PXRD showed that STA-27 remained stable until 150 °C, above which transformation to a second phase, displaying broader diffraction peaks, was observed (Figure 11).
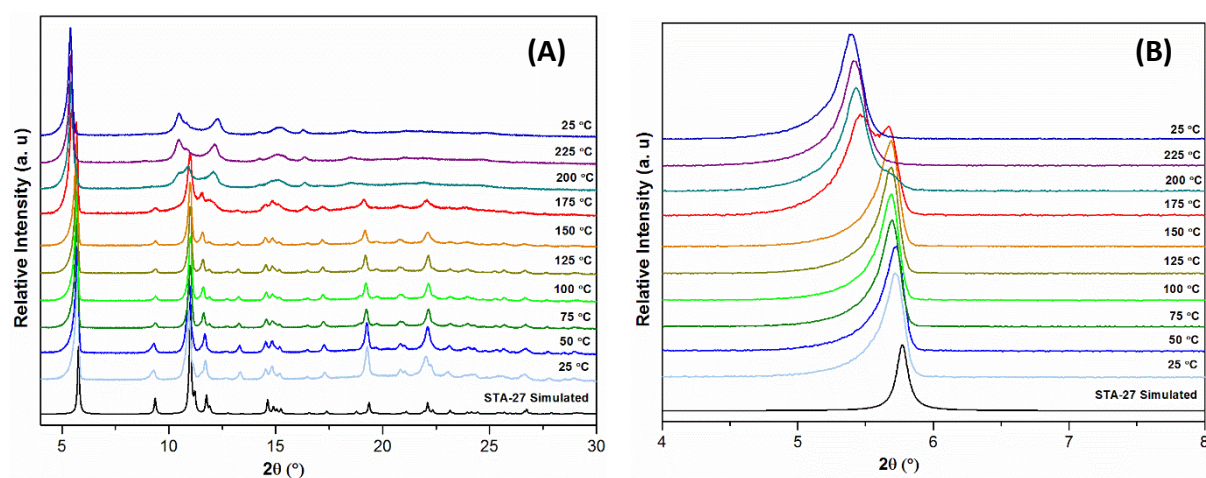

Figure 11: (A) VT-PXRD of STA-27 from 25 °C to 225 °C and cooled back to 25 °C showing phase change. (B) Zoomed in low angle view of the PXRD patterns showing the change in peak positions after 175 °C.

IR measurements were performed, heating the sample in vacuum up to 300 °C, at which temperature the STA-27 will have changed phase. Heating at 150 °C results in the removal of physically bound water and the appearance of a band at 3669 cm^{-1}, which is attributed to the hydroxyl groups (or isolated water molecules) bound at Sc^{3+} sites. Heating above this temperature results in a decrease of the intensity of this band, as chemisorbed species are removed from the Sc^{3+} coordination sphere. After heating at these temperature, CO (at -173 °C) and CD$_3$CN (at room temperature) were used as IR probes of adsorption sites in STA-27. For CO, a resonance at 2143 cm-1 that increases in samples heated to 150 °C and then decreases after heating at 200 °C is attributed to CO bound at hydroxyl groups. For CD$_3$CN, bands at 2298 cm^{-1} and 2277 cm^{-1} are assigned to CD$_3$CN binding at Sc^{3+} sites (displacing water molecules). These showed the presence of hydroxyl species upon heating the sample in vacuum at 150 °C, where the original STA-27 material is stable (Figure 11), and dosing CO and CD$_3$CN on this activated sample also indicated the presence of coordinatively unsaturated Sc^{3+} (Figure 12).
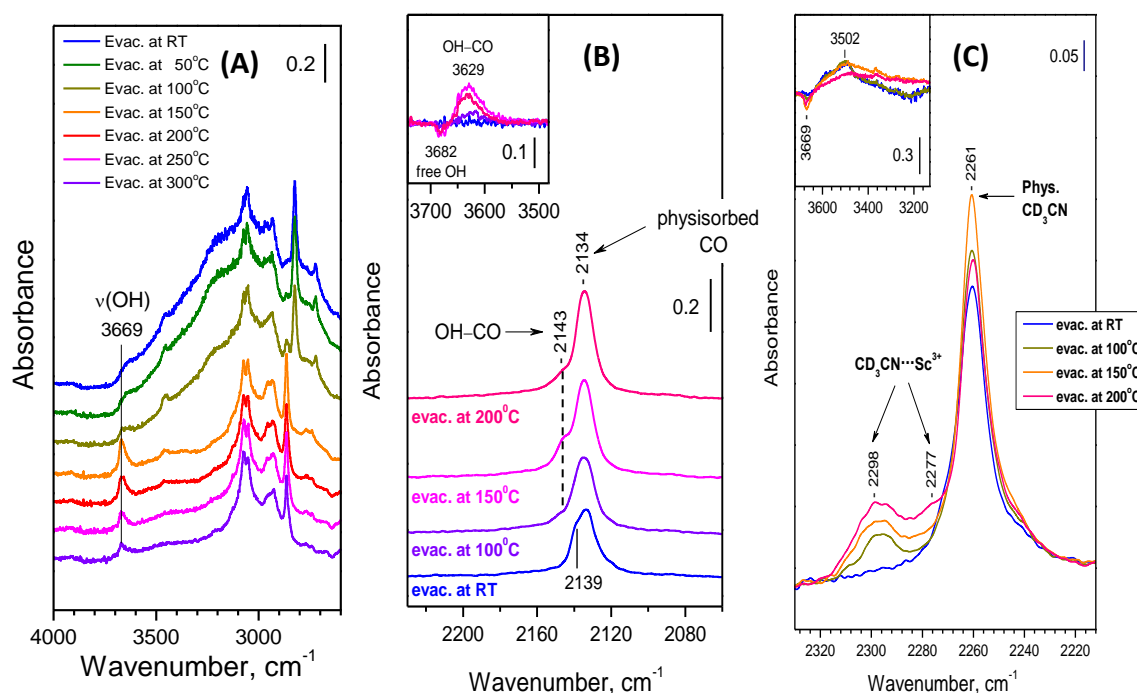

Figure 12: (A) IR spectra of STA-27 upon heating in vacuum at elevated temperatures. (B) IR spectra of CO adsorbed on the STA-27 sample pre-heated in vacuum at different temperatures. (C) IR spectra of STA-27 pre-heated in vacuum at different temperatures upon dosing with CD$_3$CN showing the presence of coordinatively unsaturated metal sites.

N$_2$ and CO$_2$ gas adsorption was performed on a sample of STA-27 activated under vacuum at 150 °C to determine its permanent porosity. Moderate uptakes were achieved in each case (N$_2$, -196 °C, 0.1 bar, 8.2 mmol g^{-1}; CO$_2$, 25 °C, 1.6 mmol g^{-1} at 1 bar and 3.1 mmol g^{-1} at 5 bar; Figures 13A and 13B). The observed N$_2$ uptake of STA-27 was comparatively less than that predicted by grand canonical Monte Carlo (GCMC) simulation (10.5 mmol g^{-1} at 0.1 bar), suggesting some loss of accessible porosity upon heating and evacuation.
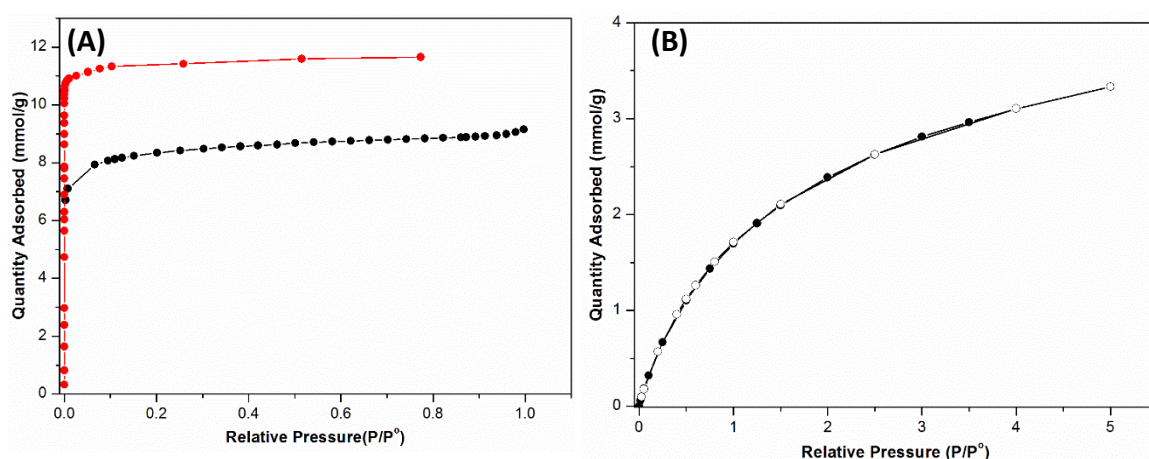

Figure 13: (A) N$_2$ adsorption isotherm at -196 °C for STA-27(black) with the GCMC simulated isotherm of STA-27 from the crystal structure (red). (B) CO$_2$ adsorption isotherm at 25 °C for STA-27.

Single crystals obtained after heating STA-27 at 225 °C in N$_2$ and then being left to stand in laboratory air for 4 days showed uniform birefringence under crossed polars in the optical microscope (Figure 14A) and so were examined by SCXRD in spite of the broad peaks observed by PXRD (Figure 14B). Remarkably, despite the relatively low quality of the data, it was possible to obtain a crystal structure of this heated material, denoted STA-27-*C* (C for calcined), in the orthorhombic space group *Pmna* (Table 1, Figure 15). Projection of this structure down the z-axis shows the same arrangement of ScO$_6$ octahedra and TCPP linkers as the parent material, but there are important differences that are most clearly illustrated by views along y-axis (Figure 15). The ScO$_6$ octahedra in STA-27-*C* are isolated, linked along the z-axis by bridging carboxylate groups from the TCPP linkers. Each Sc^{3+} atom is still coordinated by four carboxylate O atoms and a terminal O ligand but the corner-sharing O atom is now replaced by two O atoms and the difference Fourier analysis reveals additional scattering between them. The exact

nature of this species is unclear, but our model has a bicarbonate species bridging adjacent Sc^{3+} cations which we speculate forms upon exposure of the heated sample to air. The thermal decomposition of the scandium dimer through breaking of the Sc-O-Sc linkage is unambiguous, however, and results in a phase change that is likely to be topotactic.
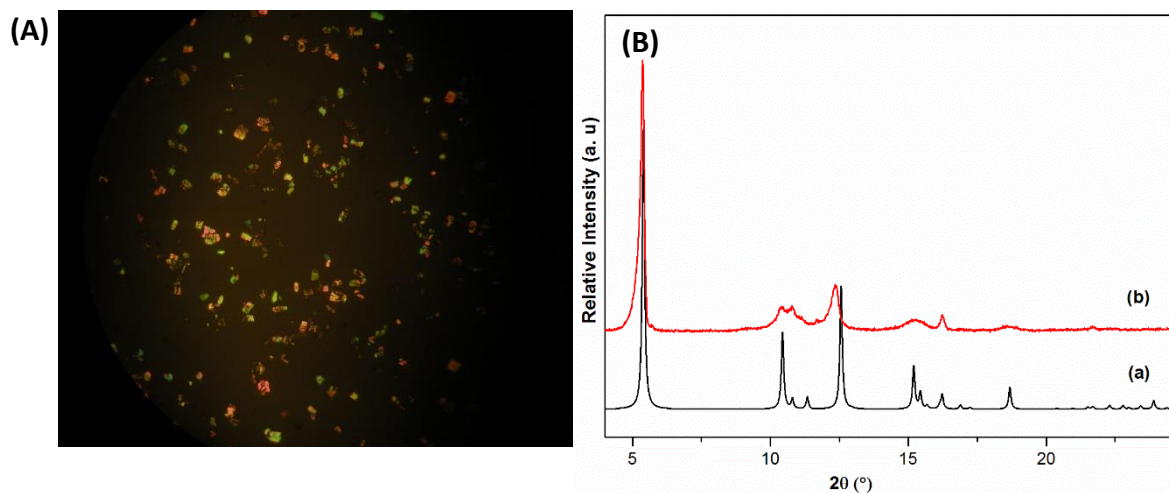
Figure 14: (A)Optical micrograph of single crystals of STA-27-*C*. (B) Simulated pattern of (a) STA-27-*C* compared with the PXRD pattern of (b) STA-27-*C* after VT-PXRD.

Figure 15: Crystal structure of STA-27-*C*.(A) 1D rod SBU of STA-27-*C*, (B) two distinct diamond shaped pore channels of STA-27-*C* viewed along the z-axis,(C) STA-27-*C* viewed along the y-axis, (E) STA-27-*C* viewed along the x-axis. Hydrogen atoms are omitted for clarity. Colour codes: Sc, Lavender; N, Sky; C, Black, O; red.

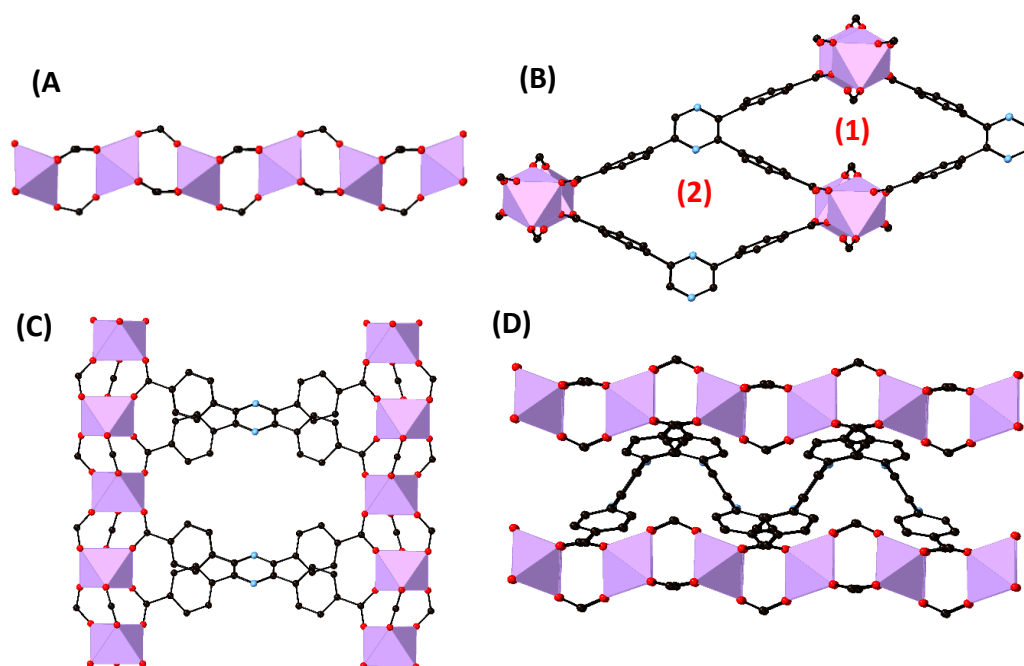Further information on the nature of the transformation comes from the ^{45}Sc MAS NMR (Figure 16). The heated sample shows two resonances, an intense sharp peak with an isotropic chemical shift of -50 ppm together with abroad resonance o much lower intensity. Upon plotting the mean ^{47}Sc isotropic shift $<\delta_{iso}>$ and qudarupolar product $<P_Q>$ for STA-27 before and after heating along with a series of Sc MOFs with different Sc coordination motifs, it was found that the value observed for STA-27 heated was near to the isolated octahedra in agreement with the data obtained from SCXRD (Figure 9). N$_2$ adsorption of STA-27-*C* at -196 °C showed considerable reduction in porosity, which we attribute to the poor uptake due to the loss of crystallinity resulting from the phase transition (Figure S6).
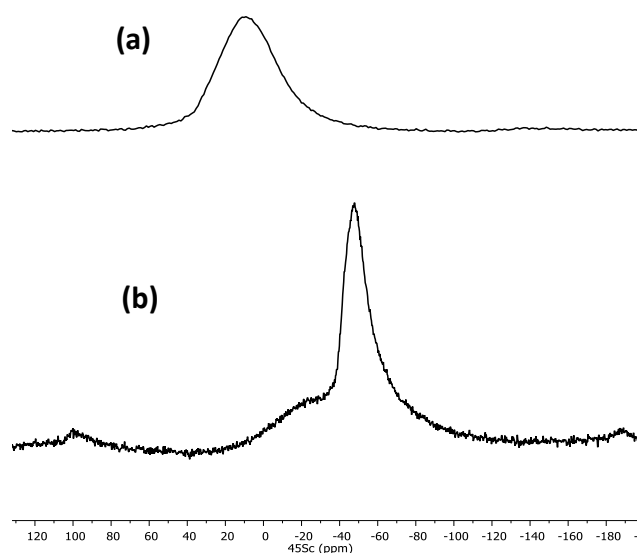

(a)

(b)

120 100 80 60 40 20 0 -20 -40 -60 -80 -100 -120 -140 -160 -180 -
45Sc (ppm)

Figure 16: (A) ^{45}Sc MAS NMR activated of (a) STA-27 and (b) STA-27-*C* .

STA-27 pre-heated at 120 °C was found to be a highly active Lewis acidic catalyst for Friedel-Crafts Michael addition reactions, imine condensation and carbonyl ene reaction where its performance is comparable with that of MIL-100(Sc) (Table 3-5).[12d] STA-27 recovered after catalysis retained its crystalline nature as shown by PXRD (Figure 17). STA-27 retained its crystalline nature over five catalytic cycles when tested for imine condensation with slight decrease in the catalytic activity in each cycle (Figure S7). This loss in catalytic activity can be due to mass loss in repeated recycling and activation or due to substrate species occupying the pores.

Table 3: Conjugate addition of 2-methylindole to methyl vinyl ketone[a]
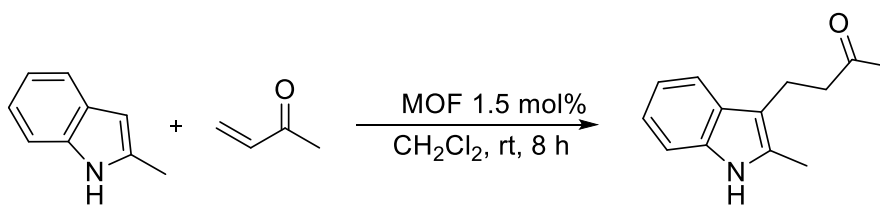
Entry	Catalyst	Product[b](%)
1	No Catalyst	2
2	STA-27	70
3	MIL-100(Sc)	74

[a] Reaction conditions: 1mmol of 2-methylindole, 1mmol of methyl vinyl ketone, 0.5 mmol of 1-methylnapthalene and 1.5 mol % catalyst was added to 5 mL DCM and stirred at room temperature for 8 h. The mol% is calculated according to the molecular weight based on a formula unit containing one Sc-O cluster. [b]Conversion was determined by ^{1}H NMR using 1-methylnapthalene as the internal standard.

Table 4: Imine condensation between 4'-fluoroacetophenone and benzylamine[a]
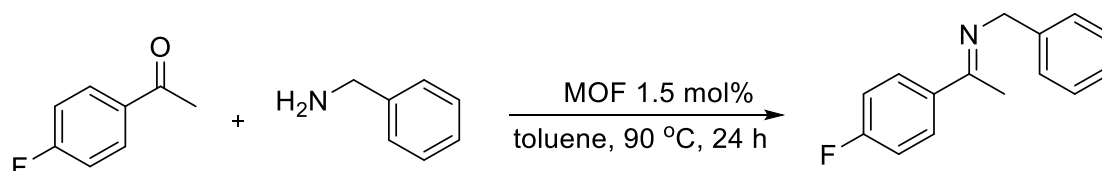
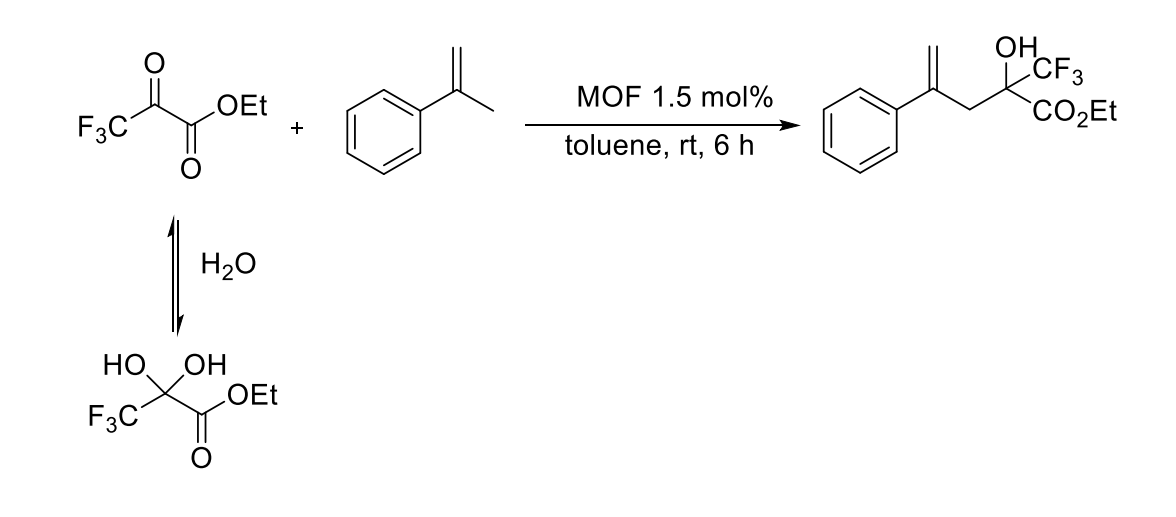| Entry	Catalyst	Product[b](%)
1	No Catalyst	2
2	STA-27	83
3	MIL-100(Sc)	80

Reaction conditions: 1mmol of 4'-fluoroacetophenone, 1.3 mmol of benzyl amine, 0.5 mmol of 1-methylnapthalene and 1.5 mol % catalyst was added to 5 mL toluene and heated at 90 °C for 24 h. [b]Conversion was determined by ^{1}H NMR using 1-methylnapthalene as the internal standard.

Table 5: Carbonyl ene reaction between ethyl trifluoropyruvate and α-methylstyrene[a]

Entry	Catalyst	Product[b](%)
1	No Catalyst	2
2	STA-27	68
3	MIL-100(Sc)	75

[a] Reaction conditions: 2.25 mmol of ethyl trifluoropyruvate, 2.7 mmol of α-methylstyrene, 0.5 mmol of 1-methylnapthalene and 1.5 mol % catalyst was added to 5 mL toluene and stirred at room temperature for 6 h. [b] Conversion was determined by ^{1}H NMR using 1-methylnapthalene as the internal standard.
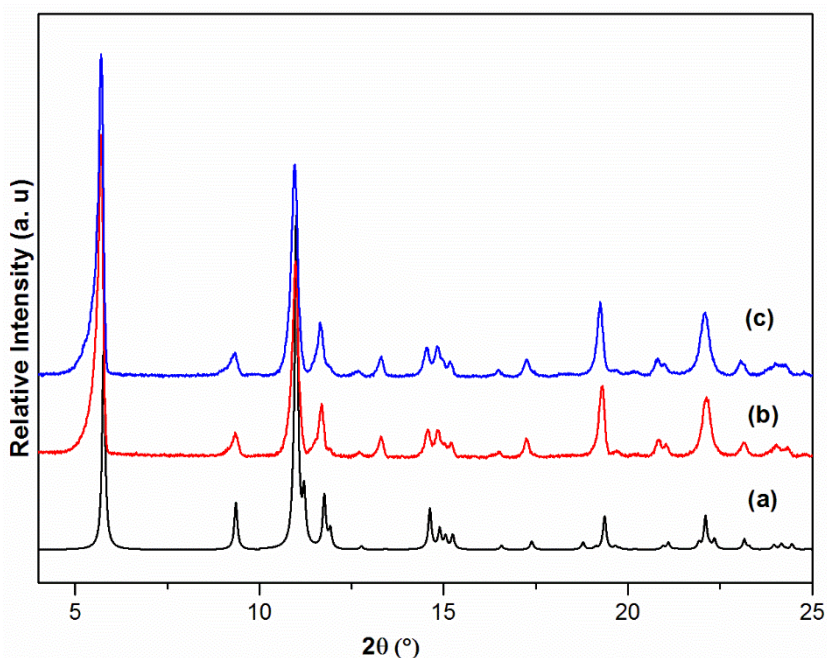

Figure 17: (a) Simulated pattern of STA-27 with the PXRD patterns of (b) STA-27 before catalysis and (c) STA-27 recovered after imine condensation reaction. STA-27 was filtered, washed multiple times with toluene followed by methanol before drying at 100 °C overnight prior to PXRD measurements.

In contrast to the high activity of STA-27, STA-27-*C* was found to be less active. For example, while STA-27 showed up to 83 % conversion in the imine condensation between 4'-fluoroacetophenone and benzylamine, STA-27-*C* showed only 36 %. The loss of crystallinity resulted from the phase transition presumably reduced the accessibility to potential Lewis acidic Sc^{3+} sites in the framework for substrate molecules, and hence decreasing the catalytic activity of the MOF.

Conclusions

A series of MOFs have been prepared using trivalent metal cations of different ionic radii (Al^{3+}, Ga^{3+} and Sc^{3+}) and the tetracarboxylic acid TCPP, which is readily formed via a two-step synthesis using inexpensive reagents. Al and Ga form $M_2(OH)_2TCPP$, which is isostructural to a previously reported $Al_2(OH)_2TCPB$, as might have been expected from the similarity of the linker. Investigation of the Al form shows that it is a thermally stable MOF which possess CO_2 adsorption performance.

Using $ScCl_3 \cdot 6H_2O$ as the metal source and TCPP as the linker in a mixed solvent system of DMF, CH_3CN and 3.5 M aq. HNO_3, gives a new Sc MOF, STA-27. Unlike the Al and Ga form, which possess a metal-based 1D rod SBU of infinite corner-sharing octahedra STA-27 possesses a 1D rod SBU not previously observed in trivalent metal MOFs. In this rod, corner-sharing dimers of two ScO_6 octahedra (with Sc_2O_{11} formula) are linked to give a MOF that possess two distinct types of parallel diamond-shaped channels. The material is an active reusable catalyst for organic C-C and C=N forming reactions and Sc^{3+} cations that have had water molecules displaced from their octahedral coordination shell are thought to be the active Lewis acid sites. The activity is comparable to that reported for MIL-100(Sc). Upon heating at 200 °C and above, STA-27 transforms to a different STA-27-*C*, in which the dimeric Sc_2O_{11} units present in the rods rearrange to isolated ScO_6 octahedra, as shown by X-ray diffraction and solid-state NMR. The topotactic transformation results in some loss of crystallinity and a reduction in pore volume and catalysis activity.

References

1 a) H. Furukawa, K. E. Cordova, M. O'Keeffe and O. M. Yaghi, *Science.*, 2013, **341**, 1230444; b) H. -C. Zhou, J. R. Long and O. M. Yaghi, *Chem. Rev.*, 2012, **112**, 673-674.

2 a) K. Sumida, D. L. Rogow, J. A. Mason, T. M. McDonald, E. D. Bloch, Z. R. Herm, T. H. Bae and J. R. Long, *Chem. Rev.*, 2012, **112**, 724-781.

3 a) I. A. Lázaro, S. Haddad, S. Sacca, C. O. -Tavra, D. F. -Jimenez and R. S. Forgan, *Chem.*, 2017, **2**, 561-578; b) M. H. Teplensky, M. Fantham, P. Li, T. C. Wang, J. P. Mehta, L. J. Young, P. Z. Moghadam, J. T. Hupp, O. K. Farha, C. F. Kaminski and D. F. -Jimenez, *J. Am. Chem. Soc.*, 2017, **139**, 7522-7532.

4 a) L. E. Kreno, K. Leong, O. K. Farha, M. Allendrof, R. P. Van Duyne and J. T. Hupp, *Chem. Rev.*, 2012, **112**, 1105-1125; b) M. G. Campbell, S. Liu, T. Swager and M. Dincá, *J. Am. Chem. Soc.*, 2015, **137**, 13780-13783.

5 a) J. Jiang and O. M. Yaghi, *Chem. Rev.*, 2015, **115**, 6966-6997; b) K. Manna, P. Ji, Z. Lin, F. X. Greene, A. Urban, N. C. Thacker and W. Lin, *Nature Communications.*, 2016, **7**, 1-11.

6 a) S. Bourrelly, P. L. Llewellyn, C. Serre, F. Millange, T. Loiseau and G. Férey, *J. Am. Chem. Soc.,* 2005, **127**, 13519-13521; b) C. Serre, F. Millange, C. Thouvenot, M. Noguès, G. Marsoller, D. Louër and G. Férey, *J. Am. Chem. Soc.*, 2002, **124**, 13519-13526; c) S. Couck, J. F. M. Denayer, G. V. Baron, T. Rémy, J. Gascon and F. Kapteijn, *J. Am. Chem. Soc.*, 2009, **131**, 6326-6327; d) C. Volkringer, T. Loiseau, N. Guillou, G. Férey, E. Elkaïm and A. Vimont, *Dalton Trans.*, 2009, **0**, 2241-2249.; e) T. Ahnfeldt, D. Gunzelmann, T. Loiseau, D. Hirsemann, J. Senker, G. Férey and N. Stock, *Inorg. Chem.*, 2009, **48**, 3057-3064; f) F. –X. Coudert, A. U. Ortiz, V. Haigis, D. Bousquett, A. H. Fuchs, A. Ballandras, G. Weber, I. Bezverkhyy, N. Geoffroy, J. -P. Bellat, G. Ortiz, G. Chaplais, J. Patarin and A. Boutin, *J. Phys. Chem. C.*, 2014, **118**, 5397-5405.

7 a) C. Serre, F. Millange, S. Surblé and G. Férey, *Angew. Chem*. *Int. Ed.*, 2004, **43**, 6286-6289; b) S. Surblé, C. Serre, C. M. –Draznieks and G. Férey, *Chem. Commun.*, 2006, **0**, 284-286; c) P. Horcajada, F. Salles, S. Wuttke, T. Devic, D. Heurtaux, G. Maurin, A. Vimont, M. Daturi, O. David, E. Magnier, N. Stock, Y. Filinchuk, D. Popov, C. Riekel, G. Férey and C. Serre, *J. Am. Chem. Soc.*, 2011, **133**, 17839-17847.

8 a) P. Horcajada, S. Surblé, C. Serre, D. -Y. Hong, Y. -K. Seo, J. -S. Chang, J. –M. Grenéche, I. Margiolaki and G. Férey, *Chem. Commun.*, 2007, **0**, 2820-2822; b) G. Férey, C. M. -

Draznieks, C. Serre, F. Millange, J. Dutour, S. Surblé and I. Margiolaki, *Science*., 2005, **309**, 2040-2042; c) M. Latroche, S. Surblé, C. Serre, C. M. -Draznieks, P. L. Llewellyn, J. H. Lee, J. –San. Chang, S. H. Jhung and G. Férey, *Angew. Chem*., 2006, **118**, 8407-8411; d) P. L. Llewellyn, S. Bourrelly, C. Serre, A. Vimont, M. Daturi, L. Hamon, G. De Weireld, J. -S. Chang, D. -Y. Hong, Y. K. Hwang, S. H. Jhung and G. Férey, *Langmuir*., 2008, **24**, 7245-7250.

9 a) A. Sonnauer, F. Hoffmann, M. Fröba, L. Kienle, V. Duppel, M. Thommes, C. Serre, G. Férey and N. Stock, *Angew. Chem. Int. Ed*., 2009, **48**, 3791-3794; b) M. Lammert, S. Bernt, F. Vermoortele, D. E. De Vos and N. Stock, *Inorg. Chem*., 2013, **52**, 8521-8528; c) T. Wittmann, R. Siegel, N. Reimer, W. Millius, N. Stock and J. Senker, *Chem. Eur. J*., 2015, **21**, 314-323; d) A. E. Anderson, C. J. Baddeley and P. A. Wright, *Catal. Lett*., 2018, **148**, 154-163.

10 a) Y. Liu, J. F. Eubank, A. J. Cairns, J. Eckert, V. Ch Kravtsov, R. Luebke and M. Eddaoudi, *Angew. Chem*., 2007, **119**, 3342-3347; b) M. Pang, A. J. Cairns, Y. Liu, Y. Belmabkhout, H. C. Zeng and M. Eddaoudi, *J. Am. Chem. Soc*., 2012, **134**, 13176-13179; c) M. Pang, A. J. Cairns, Y. Liu, Y. Belmabkhout, H. C. Zeng and M. Eddaoudi, *J. Am. Chem. Soc*., 2013, **135**, 10234-10237; d) D. Alezi, Y. Belmabkhout, M. Suyetin, P. M. Bhatt, L. J. Weselinski, V. Solovyeva, K. Adil, I. Spanopoulos, P. N. Trikalitis, A. -H. Emwas and M. Eddaoudi, *J. Am. Chem. Soc*., 2015, **137**, 13308-13318; e) Y. Belmabkhout, R. S. Pillai, D. Alezi, O. Shekhah, P. M. Bhatt, Z. Chen, K. Adil, S. Vaesen, G. De Weireld, M. Peng, M. Suetin, A. J. Cairns, V. Solovyeva, A. Shkurenko, O. El Tall, G. Maurin and M. Eddaoudi, *J. Mater. Chem A*., 2017, **5**, 3293-3303.

11 a) S. Yang, J. Sun, A. J. Ramirez-Cuesta, S. K. Callear, W. I. F. David, D. P. Anderson, R. Newby, A. J. Blake, J. E. Parker, C. C. Tang and M. Schröder, *Nat. Chem*., 2012, **4**, 887-894; b) T. -L. Hu, H. Wang, B. Li, R. Krishna, H. Wu, W. Zhou, Y. Zhao, Y. Han, X. Wang, W. Zhu, Z. Yao, S. Xiang and M. Schröder, *Nat. Commun*. 2012, **6**, 7328; c) S. Yang, A. J. Ramirez-Cuesta, R. Newby, V. Garcia-Sakai, P. Manuel, S. K. Callear, S. I. Campbell, C. C. tang and M. Schröder, *Nat. Chem*., 2015, **7**, 12-129; d) X. Han, H. G W. Godfrey, L. Briggs, A. J. Davies, Y. Cheng, L. L. Daeman, A. M. Sheveleva, F. Tuna, E. J. L. McInnes, J. Sun, C. Drathen, M. W. George, A. J. Ramirez-Cuesta. K. M. Thomas, S. Yang and M. Schröder*, Nat. Mater*., 2018, **17**, 691-696; e) C. P. Krap, R. Newby, A. Dhakshinamoorthy, H. García, I. Cebula, T. L. Easun, M. Savage, J. E. Eyley, S. Gao, A. J.

Blake, W. Lewis, P. H. Beton, M. R. Warren, D. R. Allan, M. D. Frogley, C. C. Tang, G. Cinque, S. Yang and M. Schröder, *Inorg. Chem.*, 2016, **55**, 1076-1088.

12 a) J. P. S. Mowat, S. R. Miller, A. M. Z. Slawin, V. R. Seymour, S. E. Ashbrook and P. A. Wright, *Microporous Mesoporous Mater.*, 2011, **142**, 322-333; b) J. P. S. Mowat, V. R. Seymour, J. M. Griffin, S. P. Thompson, A. M. Z. Slawin, D. Fairen-Jimenez, T. Düren, S. E. Ashbrook and P. A. Wright, *Dalton Trans.*, 2012, **41**, 3937-3941. c) A. J. Graham, A. -M. Banu, T. Düren, A. Greenaway, S. C. McKellar, J. P. S. Mowat, K. Ward, P. A. Wright and S. A. Moggach, *J. Am. Chem. Soc.*, 2014, **136**, 8606-8613; d) L. Mitchell, B. G. -Santiago, J. P. S. Mowat, M. E. Gunn, P. Williamson, N. Acerbi, M. L. Clarke and P. A. Wright, *Catal. Sci. Technology.*, 2013, **3**, 606-617; e) L. Mitchell, P. Williamson, B. Ehrlichová, A. E. Anderson, V. R Seymour, S. E. Ashbrook, N. Acerbi, L. M. Daniels, R. I. Walton, M. L. Clarke and P. A. Wright, *Chem. Eur. J.*, 2014, **20**, 17185-17197; f) R. J. Marshall, C. T. Lennon, A. Tao, H. S. Senn, C. Wilson, D. F. -Jimenez and R. S. Forgan, *J. Mater. Chem. A.*, 2018, **6**, 1181-1187.

13 I. A. Ibarra, X. Lin. S. Yang, A. J. Blake, G. S. Walker, S. A. Barnett, D. R. Allan, N. R. Champness, P. Hubberstey and M. Schröder, *Chem. Eur. J.*, 2010, **16**, 13671-13679

14 a) S. R. Miller, P. A. Wright, C. Serre, T. Loiseau, J. Marrot and G. Férey, *Chem. Commun.*, 2005, **0**, 3850-3852; b) J. P. S. Mowat, S. R. Miller, J. M. Griffin, V. R. Seymour, S. E. Ashbrook, S. P. Thompson, D. F. -Jimenez, A. -M. Banu, T. Düren and P. A. Wright*, Inorg. Chem.*, 2011, **50**, 10844-10858; c) J. Cepeda, S. P. -Yáñez, G. Beobide, O. Castillo, E. Goikolea, F. Aguesse, L. Garrido, A. Luque and P. A. Wright, *Chem. Mater.*, 2016, **28**, 2519-2528; d) J. Cepeda, S. P. -Yáñez, G. Beobide, O. Castillo, A. Luque, P. A. Wright, S. Sneddon and P. A. Wright, *Cryst. Growth. Des.*, 2015, **15**, 2352-2363; e) A. Greenaway, B. G. -Santiago, P. M. Donaldson, M. D. Froglay, G. Cinque, J. Sotelo, S. A. Moggach, E. Shiko, S. Brandani, R. F. Howe and P. A. Wright, *Angew. Chem. Int. Ed.*, 2014, **53**, 13483-13487; f) R. S. Pillai, V. Benoit, A. Orsi, P. L. Llewellyn, P. A. Wright and G. Maurin, *J. Phys. Chem. C.*, 2015, **119**, 23592-23598 g) S. C. McKellar, J. Sotelo, A. Greenaway, J. P. S. Mowat, O. Kvam, C. A. Morrison, P. A. Wright and S. A. Moggach, *Chem. Mater.*, 2016, **28**, 466-473; h) J. Sotelo, C. H. Woodall, D. R. Allan, E. Gregoryanz, R. T. Howie, K. V. Kamenev, M. R. Probert, P. A. Wright and S. A. Moggach, *Angew. Chem. Int. Ed.*, 2015, **54**, 13332-13336.

15 a) J. Cepeda, S. P. -Yáňez, G. Beobide, O. Castillo, E. Goikolea, F. Aguesse, L. Garrido, A. Luque and P. A. Wright, *Chem. Mater.*, 2016, **28**, 2519-2528; b) J. Cepeda, S. P. -Yáňez, G. Beobide, O. Castillo, A. Luque, P. A. Wright, S. Sneddon and P. A. Wright, *Cryst. Growth. Des.*, 2015, **15**, 2352-2363.

16 I. A. Ibarra, S. Yang, X. Lin, A. J. Blake, P. J. Rizkallah, H. Nowell, D. R. Allan, N. R. Champness, P. Hubberstey and M. Schröder, *Chem. Commun.*, 2011, **47**, 8304-8306.

17 Y. Jiang, L. Sun, J. Du, Y. Liu, H. Shi, Z. Liang and J. Li, *Cryst. Growth. Des.*, 2017, **17**, 2090-2096.

18 M. Krüger, R. Siegel, A. Dreischarf, H. Reinsch, J. Senker and N. Stock, *Microporous Mesoporous Mater.*, 2015, **216**, 27-35.

19 *CrystalClear-SM Exper*t v2.1. Rigaku Americas, The Woodlands, Texas, USA, and Rigaku Corporation, Tokyo, Japan, 2015.

20 Sheldrick, G. M. *Acta Crystallogr., Sect. A*. 2015, **71**, 3-8.

21 Sheldrick, G. M. *Acta Crystallogr., Sect. C*. 2015, *71*, 3-8.

22 *CrystalStructure* v4.2. Rigaku Americas, The Woodlands, Texas, USA, and Rigaku Corporation, Tokyo, Japan, 2013.

23 Spek, A. L. *Acta Crystallogr. Sect C*. 2015, **71**, 9-18.

24 Spek, A. L. *Acta Crystallogr. Sect D*. 2009, **65**, 148-155.

25 K. J. Pike, R. P. Malde, S. E. Ashbrook, J. McManus and S. Wimperis, *Soild State Nucl. Magn. Reson.*, 2000, **16**, 203-215.

26 A. Gupta, S. Chempath, M.J. Sanborn, L.A. Clark and R.Q. Snurr, *Mol.Simul.*, 2003, **29**, 29-46.

27 S.L. Mayo, B.D. Olafson and W.A. Goddard, *J.Phys.Chem.*, 1990, **94**, 8897-8909.

28 A.K. Rappé, C.J. Casewit, K.S. Colwell, W.A. Goddard and W.M. Skiff, *J.Am.Chem.Soc.*, 1992, **114**, 10024-10035.

29 http://chem-siepmann.oit.umn.edu/siepmann/trappe/index.html.

30 G. P. M. Bignami, Z. H. Davis, D. M. Dawson, S. A Morris, S. E. Russell, D. McKay, R. E. Parke, D. Luga, R. E. Morris and S. E. Ashbrook, *Chem. Sci.*, 2018, **9**, 850-859.

31 J. Perles, M. Iglesias, C. Ruiz-Valero and N. Snejko, *Chem. Commun.*, 2003, **0**, 346-347.

32 a) Y. Qiu, H. Deng, S. Yang, J. Mou, C. Daiguebonne, N. Kerbellec, O. Guillou and S. R. Batten, *Inorg. Chem.*, 2009, **48**, 3976-3981; b) A. Schoedel, M. Li, D. Li, M. O'Keeffe and O. M. Yaghi, *Chem. Rev.*, 2016, **116**, 12466-12535.

33 V. R. Seymour, PhD Thesis, *University of St Andrews*, 2013.

34 R. Giovine, C. Volkringer, S. E. Ashbrook, J. Trébosc, D. McKay, T. Loiseau, J. -P. Amoureux, O. Lafon and F. Pourpoint, *Chem. Eur. J.*, 2017, **23**, 9525-9534.

TOC Figure